International Journal of Heat and Mass Transfer 51 (2008) 5887–5894

Contents lists available at ScienceDirect

International Journal of Heat and Mass Transfer

journal homepage: www.elsevier.com/locate/ijhmt

Iterative and direct Chebyshev collocation spectral methods for one-dimensional radiative heat transfer

Ben-Wen Li *, Ya-Song Sun, Yang Yu

Key Laboratory of National Education, Ministry for Electromagnatic Processing of Materials, P.O. Box 314, Northeastern University, Shenyang 110004, China

ARTICLE INFO

Article history:
Received 2 January 2008
Received in revised form 9 April 2008
Available online 27 June 2008

Keywords:
Radiative transfer
Chebyshev collocation spectral methods
Discrete-ordinates method

ABSTRACT

In this paper, the Chebyshev collocation spectral method for one-dimensional radiative heat transfer equation with participating media is presented; and sequentially the iterative and direct solvers are developed. Implementation of the new method shows its flexibility to complex problems: highly anisotropic and space-dependent scattering. The new solvers can provide exponential convergence in space and can capture large oscillations. Numerical results verified the high accuracy of the new method, and its competitive ability compared with other newly appeared methods.

1. Introduction

During the past two decades, lots of efforts have been made to solve the radiative transfer equation (RTE). The discrete-ordinates method (DOM) in conjunction with control volume (CV), originally proposed by Carlson and Lathrop [1] to solve neutron transport, and later was adopted to solve RTE by Fiveland [2–4], almost enjoyed the most fast developing and widely applications. Even in recent years, the new methods, approaches, or procedures for RTE in terms of whether radiation intensity or temperature appeared very frequently. The former summary or review can be found in text books [5,6]. Here the authors would like to mention some salient characteristics of most recent methods or approaches.

Gritzo and Strickland [7] presented the gridless methods for RTE which is compatible with computational fluid dynamics (CFD) even using direct numerical simulation (DNS), and recently Liu and Tan [8,9] further improved this method for radiation transfer and its combination with conduction. The similar compatibility of numerical radiative heat transfer with chemical reaction by DNS is the photon Monte Carlo method presented by Wu, Modest and Haworth [10]. Finite element (FE) methods for RTE are not a new methodology, but the least-squares FE proposed by Pontaza and Reddy [11] can provide *p*-level convergence. Other methods are the partial moment entropy approximation [12], the deterministic photon free method [13], and the LTS_N method [14].

Spectral methods can provide exponential convergence in space [15] and have been widely used to solve Navier–Stokes equations in CFD [16,17], Maxwell equations in electrodynamics [18], and magnetohydrodynamics (MHD) equations in magneto-fluids-mechanics [19,20], etc. Despite the high accuracy and efficiency of spectral methods, there are seldom applications of spectral methods in radiative heat transfer computation. The main reason may exist in that the spectral methods are not suitable to the solutions of multidimensional complex geometries. To overcome this drawback of spectral methods, the spectral element methods which combined high accuracy of spectral method and flexibility to complex geometry of finite element method, were developed [11,21]. For pure spectral methods, the three works related to radiative transfer appeared in [22–24]. However, all these three works are not really correlated with "heat transfer" by thermal radiation but with quantum physics [22] or electromagnetic wave propagation and scattering [23,24]. Besides this fact, their final resultant algebraic equations need to be solved are in coefficient space, in another word, spectral equations. Very recently, Aouled-Dlala et al. [25] used the finite Chebyshev transform (FCM) for the discretization of angular derivative terms in cylindrical and spherical systems. According to the authors' knowledge, there is not any work on Chebyshev collocation methods for radiative heat transfer.

In the following of this paper, the Chebyshev collocation methods for 1D RTE will be presented in detail in Section 2. The discretized equations can be solved iteratively and directly, and the processes will be described in Sections 3 and 4, separately. Validations by typical cases with exact solutions and other numerical results are stated in Section 5. Finally the last section gives the conclusions and remarks.

* Corresponding author. Tel.: +86 24 83681756; fax: +86 24 83681758.
E-mail addresses: heatli@hotmail.com, heatli@epm.neu.edu.cn (B.-W. Li).

0017-9310/$ - see front matter © 2008 Elsevier Ltd. All rights reserved.
doi:10.1016/j.ijheatmasstransfer.2008.04.048

2. Chebyshev collocation method for 1D RTE

2.1. Governing equation and boundary condition

The governing equation for radiative heat transfer in absorbing-emitting and scattering gray medium in term of radiation intensity reads [5,6]

$$\Omega\cdot\nabla I(r,\Omega)+(k+\sigma)I(r,\Omega)=kI_b(r)+\frac{\sigma}{4\pi}\int_{\Omega'=4\pi}\Phi(\Omega'\to\Omega)I(r,\Omega')\,\mathrm{d}\Omega' \tag{1}$$

with boundary conditions

$$I(r,\Omega)=I^S(r,\Omega)+\varepsilon I_b(r)+\frac{\rho}{4\pi}\int_{n\cdot\Omega'}I(r,\Omega')\,\mathrm{d}\Omega' \tag{2}$$

where all the symbols' explanations are referred to [11].

The anisotropic scattering phase function in Eq. (1), $\Phi(\Omega'\to\Omega)$, in term of direction cosine μ is defined by

$$\Phi(\mu'\to\mu)=K(\mu',\mu)=\sum_{l=0}^{L}d_lP_l(\mu)P_l(\mu'),\quad d_0=1 \tag{3}$$

where $P_l(\mu)$ are Legendre polynomials and d_l are specified corresponding coefficients, and $L=0$ corresponds to isotropic scattering.

The one-dimensional DOM form of Eq. (1) gives

$$\mu^m\frac{\partial I^m(x)}{\partial x}+\beta(x)I^m(x)=\frac{\sigma(x)}{2}\sum_{m'=0}^{M}K(\mu^{m'},\mu^m)I^{m'}(x)w_{m'}+k(x)I_b(x),\quad\forall m \tag{4}$$

where $\beta(x)=k(x)+\sigma(x)$, is called extinction coefficient.

2.2. Chebyshev collocation spectral formulation

For Eq. (4), M directions, $\{\mu^1,\mu^2,\ldots,\mu^M\}$, together with their corresponding weights, w_m ($m=1,2,\ldots,M$), are selected to discretize the angular dependent intensity, while for space discretization, the Chebyshev collocation spectral method will be used. Similar as in [11], the strategy of the RTE discretization in this article belongs to the category of so called space-angle decoupling.

First, the mapping of arbitrary interval $[X_1,X_2]$ to standard interval $[-1,1]$ is needed to fit the requirement of Chebyshev polynomial

$$s=\frac{2x-(X_2+X_1)}{X_2-X_1} \tag{5}$$

After mapping Eq. (4) becomes

$$\mu^m\left(\frac{2}{X_2-X_1}\right)\frac{\partial I^m(s)}{\partial s}+\beta(s)I^m(s)=\frac{\sigma(s)}{2}\sum_{m'=1}^{M}K(\mu^{m'},\mu^m)I^{m'}(s)w_{m'}+k(s)I_b(s),\quad m=1,2,\ldots,M \tag{6}$$

The Gauss–Lobatto collocation points [16,17,26] are used for spatial discretization

$$s_i=\cos\frac{\pi i}{N},\quad i=0,1,\ldots,N \tag{7}$$

The Chebyshev approximation of radiative intensity reads

$$I_N^m(s)=\sum_{k=0}^{N}\hat{I}_k^mT_k(s) \tag{8}$$

where the $T_k(s)$ is the first kind Chebyshev polynomial, the coefficients $\hat{I}_k^m$, $k=0,1,\ldots,N$ are determined by requiring $I_N^m(s)$ to coincide with $I^m(s)$ at the collocation points s_i, $i=0,1,\ldots,N$, and the polynomial of degree N defined by Eq. (8) can be the Lagrange interpolation polynomial based on the set $\{s_i\}$ like

$$I_N^m(s)=\sum_{j=0}^{M}h_j(s)I^m(s_j) \tag{9}$$

with $I_N^m(s)=I^m(s_j)$, and $h_j(s)$ is the polynomial of degree N and is a function of the first order derivative of Chebyshev polynomial. Its detail definition and expression can be found in [17].

The representation Eq. (9) is equivalent to Eq. (8) and will be used in our formulations to avoid spectral coefficients solution, and further to avoid fast cosine transformation.

After substitution of derivative matrices in s [16,17,26], the discretized form of Eq. (6) reads

$$\sum_{k=0}^{N}\mathbf{A}_{ik}^m\mathbf{I}_k^m+\sum_{k=0}^{N}\mathbf{B}_{ik}\mathbf{I}_k^m=\mathbf{f}_i^m,\quad m=1,2,\ldots,M \tag{10}$$

where

$$\mathbf{A}_{ik}^m=\mu^m\left(\frac{2}{X_2-X_1}\right)\mathbf{D}_{s,ik}^{(1)} \tag{11}$$

$$\mathbf{B}_{ik}=\begin{cases}\beta(s_i), & i=k\\ 0, & \text{otherwise}\end{cases} \tag{12}$$

$$\boldsymbol{f}_i^m=\frac{\sigma(s_i)}{2}\sum_{m'=1}^{M}K(\mu^{m'},\mu^m)\boldsymbol{I}^{m'}(s_i)w_{m'}+k(s_i)\boldsymbol{I}_b(s_i) \tag{13}$$

and $\mathbf{D}_{s,ik}^{(1)}$ is the first order derivative matrix in s direction corresponding to Gauss–Lobatto collocation points and its detail computation can be found in [16,17,26].

Eq. (10) is valid for all directions, and for each direction m, the matrices $\boldsymbol{A}$ and $\boldsymbol{B}$ have the same size and can be incorporated into one matrix. Thereafter Eq. (10) can be rewritten as

$$\sum_{k=0}^{N}\mathbf{C}_{ik}^m\mathbf{I}_k^m=\mathbf{f}_i^m,\quad m=1,2,\ldots,M \tag{14}$$

where $\boldsymbol{C}_{ik}^m=\boldsymbol{A}_{ik}^m+\boldsymbol{B}_{ik}$.

Eq. (14) has to be solved with appropriate boundary conditions. The boundary conditions, whether they are of Dirichlet or Neumann type, can easily be imported and the detail can be found in text book like [15–17,26].

We finally rewrite Eq. (14) as following after boundary conditions import

$$\mathbf{C}^m\mathbf{I}^m=\mathbf{F}^m,\quad m=1,2,\ldots,M \tag{15}$$

3. Iterative solver

From the above formulations we know that the unknown vector $\boldsymbol{I}^m$ is also included in the right hand side of Eq. (15). The intuitive decision is to solve it iteratively. The implementation of iterative solver for Eq. (15) can be carried out according to the following routine:

Step 1: Import boundary conditions.
Step 2: Give $\boldsymbol{I}^m$ an initial assumption (zero for example) in all directions except for boundary conditions.
Step 3: Compute $\boldsymbol{F}^m$ according to Eq. (13).
Step 4: Directly solve Eq. (15) by $\boldsymbol{I}^m=(\boldsymbol{C}^m)^{-1}\boldsymbol{F}^m$ for all m.
Step 5: Compare the newly solved $\boldsymbol{I}^m$ with their initial assumption or former iteration values for all directions and nodes and find the maximum absolute difference.
Step 6: Terminate the iteration if the maximum absolute difference is less than the tolerance (10^{-12} for example), otherwise go back to step 3.

In principle, there are no obstacles to execute this routine. However, great care should be taken in choosing the number of nodes, N. Because the matrix $\boldsymbol{A}$ related to the first order derivative matrix $\boldsymbol{D}$, corresponding to Chebyshev Gauss–Lobatto collocation points, can be ill-conditioned with its elemental values being as large as 10^{14} [17]. The detail discussions concerned with condition number and spectral radius are referred to [17,26,27].

4. Direct solver

For Eq. (15), direct solution is certainly more attractive due to the high efficiency when the computer memory is sufficient.

First, assemble all directional radiative identities into to one large vector

$$\boldsymbol{I} = (I_0^1, I_1^1, \ldots, I_N^1, \ldots, I_0^M, I_1^M, \ldots, I_N^m)^{\mathrm{T}} \tag{16}$$

Accordingly, the vector $\boldsymbol{F}^m$, being of the right hand side of Eq. (15), is also reconstructed to be of rectangular matrix which thereafter is free of up index

$$\boldsymbol{F}(s) = \boldsymbol{H}\boldsymbol{I} \tag{17}$$

$$\boldsymbol{H} = \begin{bmatrix} \boldsymbol{H}^1 \\ \vdots \\ \boldsymbol{H}^M \end{bmatrix} \tag{18}$$

where

$$\boldsymbol{H}^m = \begin{bmatrix} \boldsymbol{H}^{m,1} & \boldsymbol{H}^{m,2} & \cdots & \boldsymbol{H}^{m,M} \end{bmatrix} \tag{19}$$

and

$$\boldsymbol{H}^{m,j} = \mathrm{diag}(h_0^{m,j}, \ldots, h_N^{m,j}) \tag{20}$$

hence

$$h_i^{m,j} = \frac{\sigma(s_i)}{2} w_j K(\mu^m, \mu^j) + k(s_i) I_b(s_i) \tag{21}$$

Afterward, Eq. (15) becomes

$$\boldsymbol{C}\boldsymbol{I} = \boldsymbol{H}\boldsymbol{I} \tag{22}$$

where

$$\boldsymbol{C} = \mathrm{diag}(\boldsymbol{C}^1, \ldots, \boldsymbol{C}^M) \tag{23}$$

Keep in mind that, Eq. (22) is not the final form for direct solver because the boundary conditions have not been imported yet, and of course it will give unique solutions for preferred cases in which the boundary conditions are specified, as can be known in the next section.

5. Numerical results

To verify our spectral solvers for 1D RTE, three examples are adopted. The first example, which is copied from [11], is mainly used to test the accuracy of the method in the case of a localized sharp gradient of intensity. The second example is used mainly to test the suitability for large oscillations, and it is copied from [28]. The last one is much complicated with space-dependent albedo and highly anisotropic scattering [29].

5.1. Example 1: transparent boundaries, no incident radiation, isotropic scattering medium within bi-unit strip

To show the exponential space convergence of Chebyshev collocation method for 1D RTE, a problem considering transparent boundaries, no incident radiation, and isotropic scattering medium within bi-unit strip is adopted [11]. Its modeled equation is

$$\mu \frac{\partial I(x,\mu)}{\partial x} + I(x,\mu) = f(x,\mu) \text{ in } [X_1, X_2] \times \Omega = [-1,1] \times \Omega \tag{24}$$

with boundary conditions

$$I(-1,\mu) = I(1,\mu) = 0 \tag{25}$$

Giving a prescribed forcing function

$$f(x,\mu) = \sin(\pi\mu)[\mu\pi\cos(\pi x) + \sin(\pi x)] \tag{26}$$

The analytic solution of Eq. (24) is given by $I(x,\mu) = \sin(\pi x)\sin(\pi\mu)$ under such conditions.

Here we used the S_2 approximation [5,6] for angular discretization, and $\mu = 0.5773503$. Similar as in many references for spectral methods applications, here three measures [30] are used to estimate the errors of our solvers.

$$\varepsilon_{\mathrm{MAX}} = \max \|I_i - I_i^{\mathrm{exact}}\| \tag{27}$$

$$\varepsilon_{\mathrm{MSQ}} = \sqrt{\frac{\sum_{i=1}^{N-1}(I_i - I_i^{\mathrm{exact}})^2}{(N-1)}} \tag{28}$$

$$\varepsilon_{\mathrm{L}}^2 = \sqrt{\frac{\sum_{i=1}^{N-1}(I_i - I_i^{\mathrm{exact}})^2}{\sum_{i=1}^{N-1}(I_i^{\mathrm{exact}})^2}} \tag{29}$$

These three errors against resolutions for example one are list in Table 1. Obviously one can see that the spectral solver can provide very high accuracy and the errors' decrease show the exponential trends.

5.2. Example 2: Gaussian shaped radiative source term between 1D parallel black slab

Capture the large oscillations of problems is an important index for numerical methods. Here we adopt the example [28] with Gaussian shaped radiative source term and nonscattering medium. This problem provides a very large nonphysical oscillation and its modeled equation is

$$\mu \frac{\partial I(x,\mu)}{\partial x} + kI(x,\mu) = \mathrm{e}^{-(x-c)^2/\alpha^2}, \quad [X_1, X_2] \times \Omega = [0,1] \times \Omega \tag{30}$$

with boundary conditions

$$I(0,\mu) = k^{-1}\mathrm{e}^{-c^2/\alpha^2}, \quad \mu > 0 \tag{31a}$$

$$I(1,\mu) = k^{-1}\mathrm{e}^{-(1-c)^2/\alpha^2}, \quad \mu < 0 \tag{31b}$$

The analytic solution of Eq. (30) in the case of $\mu > 0$ is given by

$$\begin{aligned} I(x,\mu) = {} & I(0,\mu)\exp\left(-\frac{kx}{\mu}\right) - \frac{\alpha\sqrt{\pi}}{2\mu} \\ & \times \exp\left\{-\frac{k}{\mu}\left[x - \left(\frac{\alpha^2 k}{4\mu} + c\right)\right]\right\} \\ & \times \left[\mathrm{erf}\left(\frac{\alpha k}{2\mu} + \frac{c-x}{\alpha}\right) - \mathrm{erf}\left(\frac{\alpha k}{2\mu} + \frac{c}{\alpha}\right)\right] \end{aligned} \tag{32}$$

Using our direct solver to the case of $c = 0.5$, $\alpha = 0.02$, $\mu = 1.0$, and an optical thickness of $\tau_{\mathrm{L}} = kx = 0.1$. The results against three different resolutions are shown in Fig. 1.

Table 1
MAX, MSQ and L^2 errors of the spectral solver for example 1

N	$\varepsilon_{\mathrm{MAX}}$	$\varepsilon_{\mathrm{MSQ}}$	ε_{L^2}
5	10^{-2}	10^{-2}	10^{-2}
9	10^{-5}	10^{-5}	10^{-5}
13	10^{-9}	10^{-9}	10^{-9}
17	10^{-13}	10^{-13}	10^{-13}
21	10^{-15}	10^{-15}	10^{-16}

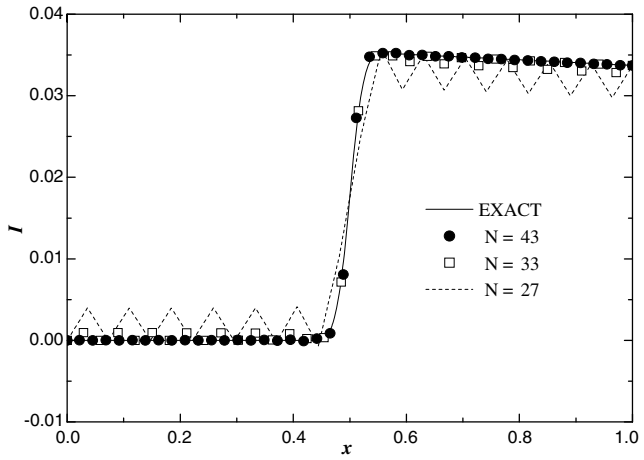

Fig. 1. Distribution of radiative intensity with different resolutions for example 2.

Fig. 1 shows that when the resolution is up to 43, our results agree well with the exact solution and the oscillation in the middle is captured. The authors like to mention that, the nodes of Chebyshev collocation are clustered on two ends due to the intrinsic characteristic of Chebyshev collocation points, but the oscillation happened in the middle. So we used the grids transform [31] and gave uniform spacing grids in this example.

5.3. Example 3: anisotropic and space-dependent scattering medium with incident radiation within 1D parallel planes

From previous two examples we know that only the direct spectral solver is needed up to now because the unknown radiative intensities are not included in the right hand side of discretized RTE and only one direction cosine is used. From practical sense, more complicated cases may appear such as anisotropic scattering. Now one such typical example [29] is adopted in which the anisotropic and space-dependent scattering medium is included. Its 1D DOM governing equation is referred to Eq. (4) on the domain of $[X_1,X_2]\times\Omega=[0,1]\times[-1,1]$ but with a zero source term. The space-dependent scattering coefficient is $\sigma(x)=x$ and extinction coefficient is $\beta(x)=1$. In [29], the authors represented the albedo (the ratio of scattering coefficient to extinction coefficient) in terms of Legendre polynomials, and solved the forward and backward radiation intensities, and radiation fluxes analytically. Now the cases together with their results are used as benchmark in many references. Same as in [11], two cases of external irradiation at a boundary are considered, namely, isotropic incidence and anisotropic incidence.

This time the S_8 approximation [6] is used for angular discretization with the discrete-ordinates as $\{-0.897327,\ -0.593795,\ -0.406205,\ -0.102672,\ 0.102672,\ 0.406205,\ 0.593795,\ 0.897327\}$ and corresponding weights $w_m=0.25$. In order to check the influences of discrete-ordinates number on results, the S_{10} approximation is used also. The discrete-ordinates and corresponding weights for S_{10} can be found in [6]. The medium has a forward scattering with $L=7$ and $d_l=\{1.0,\ 1.98398,\ 1.50823,\ 0.70075,\ 0.23489,\ 0.05133,\ 0.00760,\ 0.00048\}$ in Eq. (3).

5.3.1. Case 1: isotropic incidence

The expressions of boundary conditions are

$$I(0,\mu)=I_1^S(0,\mu)=1 \text{ on } x=0,\quad \mu\in(0,1] \tag{33a}$$

$$I(1,\mu)=I_2^S(1,\mu)=0 \text{ on } x=1,\quad \mu\in[-1,0) \tag{33b}$$

The execution of the iterative solver for multi discrete-ordinates $M=8$ of this example is nothing different from Section 3. However, the import of boundary conditions for direct solver needs more detail description continued from Section 4.

Going back to Eq. (22), one can get the new form after boundary conditions imported

$$(\tilde{\boldsymbol{C}}-\tilde{\boldsymbol{H}})\tilde{\boldsymbol{I}}=\boldsymbol{Q} \tag{34}$$

In Eq. (34), $\tilde{\boldsymbol{I}}$ comes from Eq. (16) but the boundary node values were excluded, $\tilde{\boldsymbol{C}}$ and $\tilde{\boldsymbol{H}}$ come from Eq. (22) and include the consequently exchanges due to boundary conditions importing, and $\boldsymbol{Q}$ is an enlarged constant vector which appears also due to boundary conditions importing. Their detailed expressions are given in the following according to the present boundary conditions Eq. (33), respectively.

$$\boldsymbol{I}=(I_1^1,I_2^1,\ldots,I_N^1,\ldots,I_0^M,I_1^M,\ldots,I_{N-1}^M)^{\mathrm{T}} \tag{35}$$

$$\tilde{\boldsymbol{C}}=\mathrm{diag}(\tilde{\boldsymbol{C}}^1,\ldots,\tilde{\boldsymbol{C}}^M) \tag{36}$$

where

$$\tilde{\boldsymbol{C}}^m=\begin{cases}\boldsymbol{C}^m(1:N,1:N) & \text{if } \mu^m>0\\ \boldsymbol{C}^m(0:N-1,0:N-1) & \text{if } \mu^m<0\end{cases}$$

$$\tilde{\boldsymbol{H}}=\begin{bmatrix}\tilde{\boldsymbol{H}}^{1,1} & \tilde{\boldsymbol{H}}^{1,2} & \cdots & \tilde{\boldsymbol{H}}^{1,M}\\ \tilde{\boldsymbol{H}}^{2,1} & \tilde{\boldsymbol{H}}^{2,2} & \cdots & \tilde{\boldsymbol{H}}^{1,M}\\ \vdots & \vdots & \ddots & \vdots\\ \tilde{\boldsymbol{H}}^{M,1} & \tilde{\boldsymbol{H}}^{M,2} & \cdots & \tilde{\boldsymbol{H}}^{1,M}\end{bmatrix} \tag{37}$$

where

$$\tilde{\mathbf{H}}^{m,j}=\begin{cases}\tilde{\mathbf{H}}^{m,j}(1:N,1:N) & \text{if } \mu^m>0 \text{ and } \mu^j>0\\ \tilde{\mathbf{H}}^{m,j}(1:N,0:N-1) & \text{if } \mu^m>0 \text{ and } \mu^j<0\\ \tilde{\mathbf{H}}^{m,j}(0:N-1,1:N) & \text{if } \mu^m<0 \text{ and } \mu^j>0\\ \tilde{\mathbf{H}}^{m,j}(0:N-1,0:N-1) & \text{if } \mu^m<0 \text{ and } \mu^j<0\end{cases}$$

$$\boldsymbol{Q}=\begin{bmatrix}\boldsymbol{Q}^1\\ \boldsymbol{Q}^2\\ \vdots\\ \boldsymbol{Q}^M\end{bmatrix} \tag{38}$$

where

$$\mathbf{Q}^m=\begin{cases}\sum_{j=1}^{M/2}\mathbf{H}^{m,j}(1:N,1)I_0^j+\sum_{j=M/2+1}^{M}\mathbf{H}^{m,j}(1:N,N)I_N^j+\mathbf{C}^m(1:N,0)I_0^m\\ \quad \text{if } \mu^m>0\\ \sum_{j=1}^{M/2}\mathbf{H}^{m,j}(0:N-1,1)I_0^j+\sum_{j=M/2+1}^{M}\mathbf{H}^{m,j}(0:N-1,N)I_N^j+\mathbf{C}^m(0:N-1,0)I_N^m\\ \quad \text{if } \mu^m<0\end{cases}$$

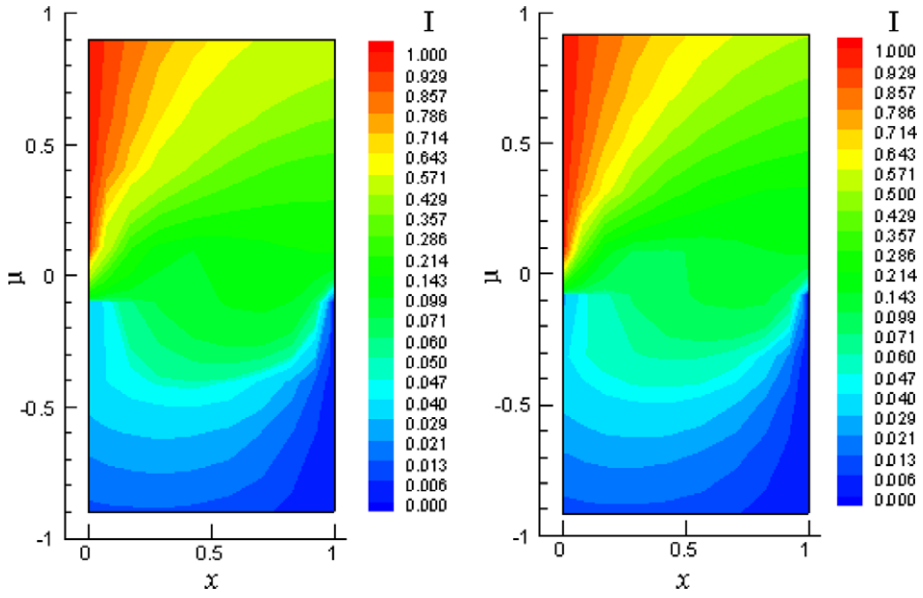

Fig. 2. Contour plot of the computed radiation intensity, $I(x,\mu)$ in space-angle domain. Case 1 of example 3. (a) S_8 for angular discretization and (b) S_{10} for angular discretization.

After the description of boundary conditions import, now we turn to the results of case 1.

Fig. 2 shows the computed contour plots of radiative intensity $I(x,\mu)$ with a resolution of $N = 11$. The left one is from S_8 for angular discretization, and the right one is from S_{10}. Compared our results with the plot (b), by space-angle coupled least-squares finite element method (LS is named in [11]), of Fig. 3 in [11], one can conclude that, our results from S_{10} are better than those from S_8, but all the present results are less accurate than those by LS. The reasons may exist as following.

As mentioned in [11], the boundary conditions implicitly allow for a sharp discontinuity in the radiation intensity angular distribution at $\mu = 0$, e.g., $I(0,0^-)$ may not be equal to $I(0,0^+)$. In [11], a double fringe of nodes at $\mu = 0$, one for $\mu = 0^-$ and the other for $\mu = 0^+$, are used to allow for such possibilities. However, in our space-angle decoupled spectral DOM (abbreviate to SP-DOM later and in figure and tables), it is impossible to do this because the DOM quadrature rule is level-symmetric, i.e., it does not contain the point $\mu^m = 0$.

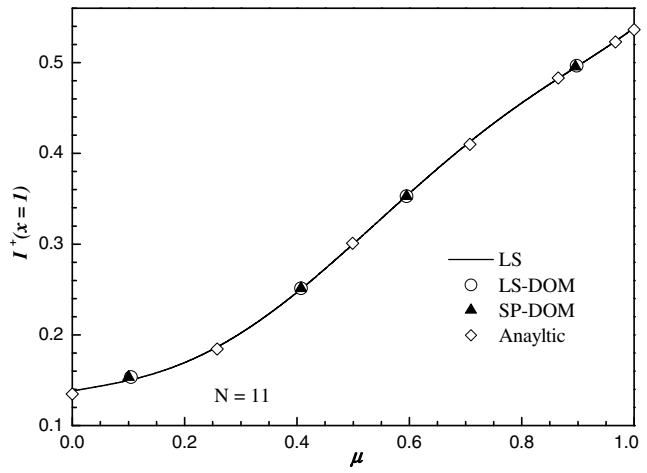

Fig. 4. Computed exit distribution of radiation intensity I^+ at $x = 1$. Case 1 of example 3.

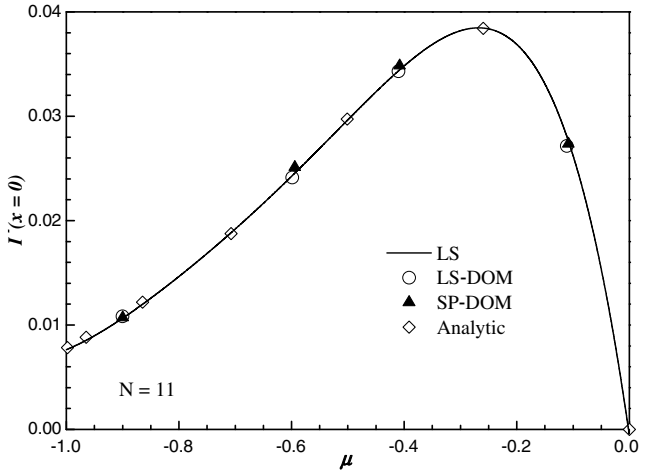

Fig. 3. Computed exit distribution of radiation intensity I^- at $x = 0$. Case 1 of example 3.

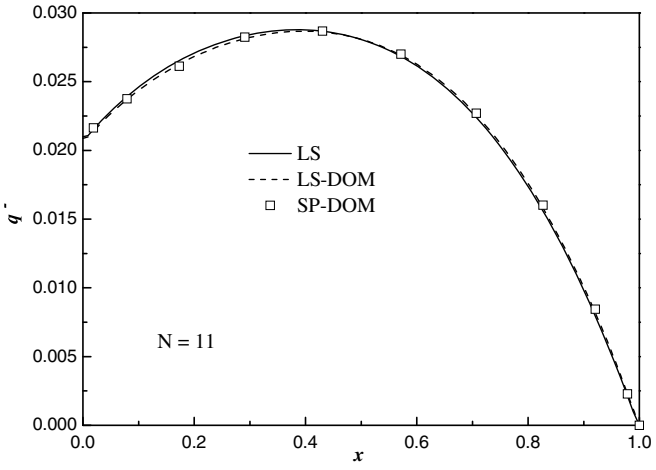

Fig. 5. Computed backward radiation heat flux distribution. Case 1 of example 3.

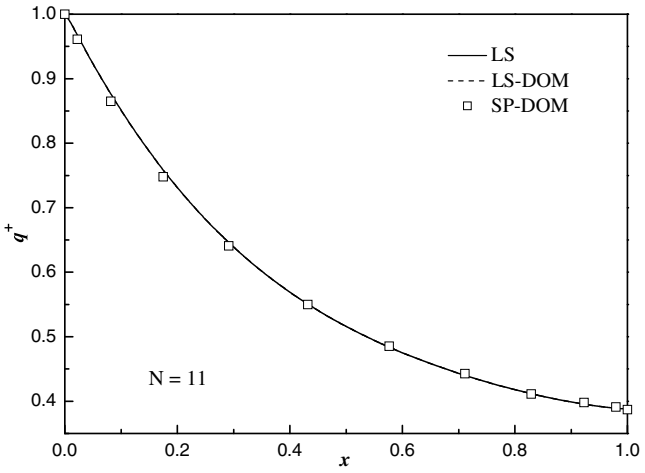

Fig. 6. Computed forward radiation heat flux distribution. Case 1 of example 3.

Table 2
Hemispherical reflectivity and transmissivity of a slab with unit thickness, transparent boundaries

	LS	LS-DOM	SP-DOM	Analytic
Reflectivity	0.020878	0.020639	0.020740	0.020878
Transmissivity	0.386094	0.386612	0.386735	0.386096

Case 1 of example 3.

Exit distributions of radiative intensity I^- at $x = 0$ and I^+ at $x = 1$ are shown in Figs. 3 and 4, respectively. For the purpose of comparison, the analytic values from [29] are plotted, and the results by LS and LS-DOM from [11] are copied. Obviously our results agree very well with those.

The backward and forward radiation heat flux distributions, q^- and q^+ are shown in Figs. 5 and 6, respectively. Similarly, the results by LS and LS-DOM from [11] are copied for comparison (this time the analytic values are unavailable). One can see that our SP-DOM almost gives the identical heat flux distributions as both LS and LS-DOM did.

Finally, the hemispherical reflectivity and transmissivity of the slab, $q^-(x = 0)$ and $q^+(x = 1)$, are compared with the analytic values [29] and results by LS and LS-DOM [11]. Table 2 also shows that our SP-DOM can provide good results.

5.3.2. Case 2: anisotropic incidence

In this case, the incident radiation at the boundary $x = 0$ arrives along specified directions, while the scattering law and space-dependent scattering coefficient remain the same as in case 1. Now the expressions of boundary conditions are complicated and as follows [11]:

$$I(0,\mu) = I_1^S(0,\mu) = g(\mu) \text{ on } x = 0,\ \ \mu \in (0,1] \tag{39a}$$

$$I(1,\mu) = I_2^S(1,\mu) = 0 \text{ on } x = 1,\ \ \mu \in [-1,0) \tag{39b}$$

where

$$g(\mu) = \begin{cases} 0, & 0.0 < \mu \leqslant 0.1 \\ \frac{1}{2}\{1 + \sin[\frac{\pi}{0.1}(\mu - 0.15)]\}, & 0.1 \leqslant \mu \leqslant 0.2 \\ 1, & 0.2 \leqslant \mu \leqslant 0.5 \\ \frac{1}{2}\{1 + \sin[\frac{\pi}{0.1}(\mu - 0.55)]\}, & 0.5 \leqslant \mu \leqslant 0.6 \\ 0, & 0.6 < \mu \leqslant 1.0 \end{cases} \tag{40}$$

which defines a piecewise constant radiation intensity distribution between 0 and 1, with smooth transitions by sine curves.

The process of boundary conditions import is the same as in case 1.

Fig. 7 shows the computed contour plots of radiative intensity $I(x,\mu)$ with a resolution of $N = 11$. Same as in case 1, the left plot is from S_8 for angular discretization, and the right one is from S_{10}. As one can see that, the left plot from S_8 for angular discretization is almost the same as the plot (b), by LS-DOM, of Fig. 8 in [11], and both of them are prone to the ray effect because the space-angle decoupled formulations act the base. On the other hand, our right plot from S_{10} is very similar to the plot (a), by LS, of Fig. 8 in [11]. Carefully comparing our right plot of Fig. 7 with the plot (a) of Fig. 8 in [11], one can find the differences. Both widths of red core part along μ axis are almost the same, but the widths of green parts on two plots are very different with ours being larger. This phenomenon can be explained that more discrete-ordinates can span more different incident directions. From this it is proved

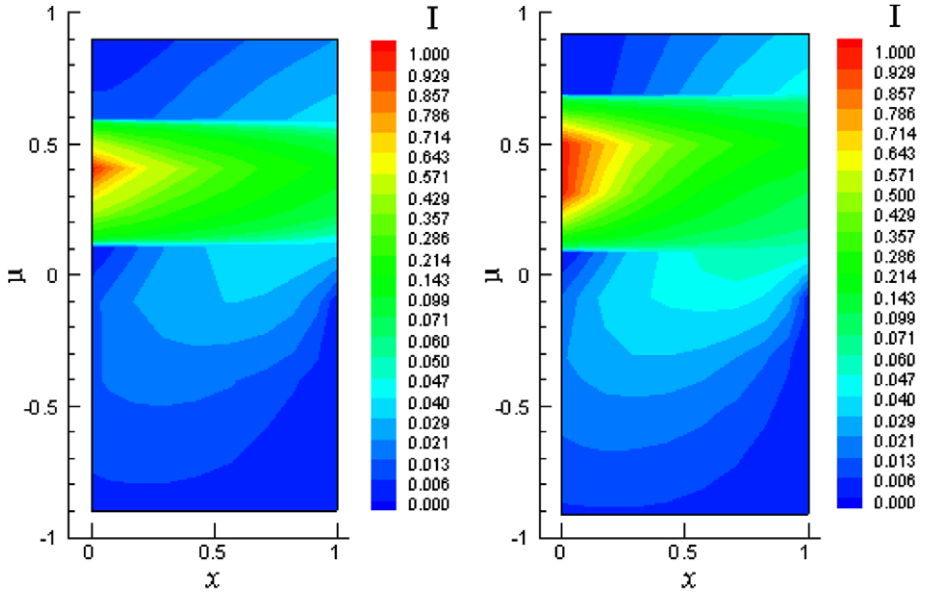

Fig. 7. Contour plot of the computed radiation intensity, $I(x,\mu)$ in space-angle domain. Case 2 of example 3. (a) S_8 for angular discretization and (b) S_{10} for angular discretization.

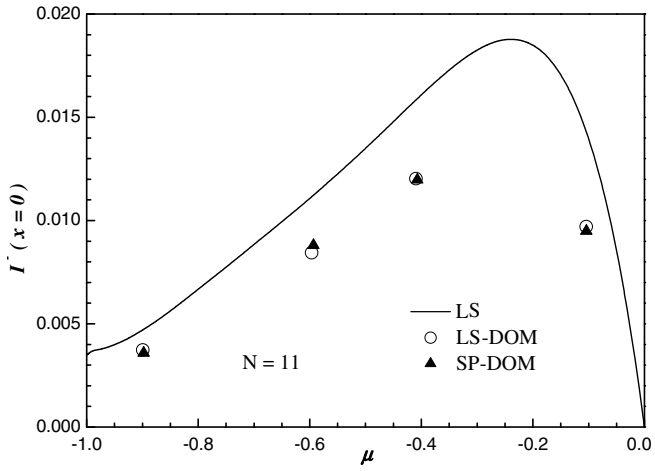

Fig. 8. Computed exit distribution of radiation intensity I^- at $x = 0$. Case 2 of example 3.

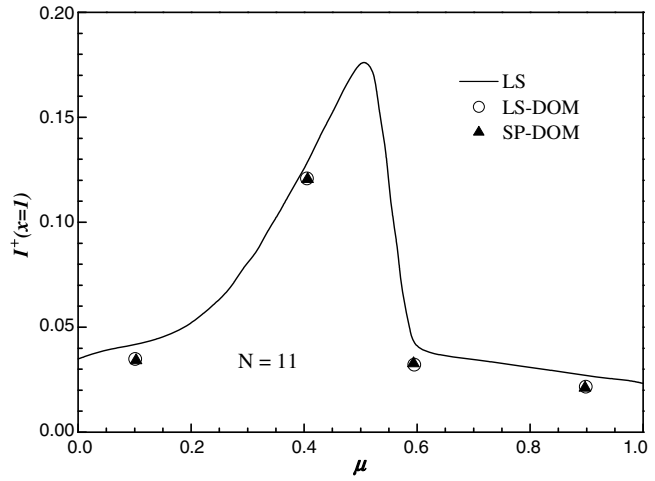

Fig. 9. Computed exit distribution of radiation intensity I^+ at $x = 1$. Case 2 of example 3.

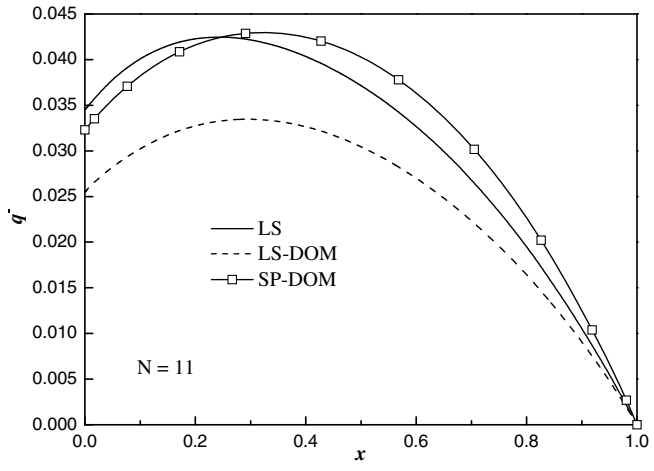

Fig. 10. Computed backward radiation heat flux distribution. Case 2 of example 3.

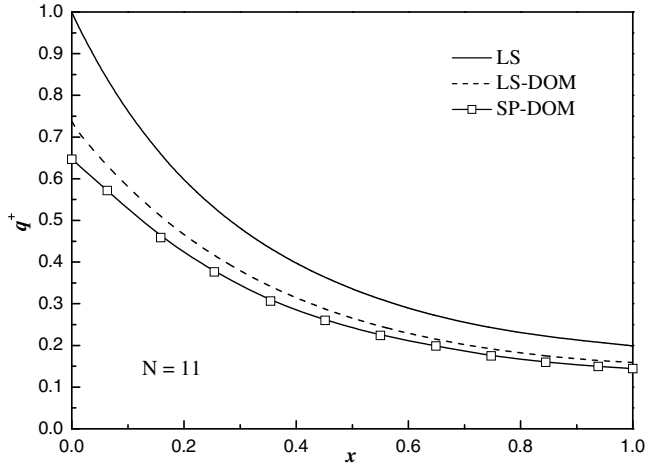

Fig. 11. Computed forward radiation heat flux distribution. Case 2 of example 3.

again that the ray effect can be mitigated by adding discrete-ordinates [32–36].

Exit distributions of radiative intensity I^- at $x = 0$ and I^+ at $x = 1$ are shown in Figs. 8 and 9 using S_8, respectively. Again the results by LS and LS-DOM from [11] are copied. This time our results are closer to the results of LS-DOM.

The backward and forward radiation heat flux distributions, q^- and q^+ are shown in Figs. 10 and 11 using S_{10}, respectively. Again the results by LS and LS-DOM from [11] are copied for comparison. The results indicate that our q^- distribution (see Fig. 10) is closer to that of LS, while our q^+ distribution (see Fig. 11) is something close to that of LS-DOM.

Finally, the hemispherical reflectivity and transmissivity of the slab, $q^-(x = 0)$ and $q^+(x = 1)$ using S_{10}, are listed and compared with those results by LS and LS-DOM [11]. Table 3 shows that the accuracy of SP-DOM is in between of LS and LS-DOM. The values of LS and LS-DOM in Table 3are listed against p-level. However, we found that the values of SP-DOM almost do not change when the resolution $N = 11$.

Our direct solver is applied to examples 1 and 2, but the both iterative and direct solvers are applied to example 3. As expected, compared with the iterative solver the direct solver can save much more CPU time as listed in Table 4. The computer we used is an Intel Pentium processor with 3.4 GHz frequency and 1.5 GB memory. In Table 4, the tolerance for iterative solver is 10^{-12} and the CPU time is the same for both cases 1 and 2 in example 3 whether using

Table 3
Hemispherical reflectivity and transmissivity of a slab with unit thickness, transparent boundaries

Formulation	p-level	Reflectivity	Transmissivity
LS	4	0.033855	0.205899
	6	0.033849	0.205897
	8	0.033849	0.205897
LS-DOM	4	0.025182	0.162091
	6	0.025290	0.162969
	8	0.025422	0.163365
SP-DOM	11 (Resolution)	0.032084	0.189536

Case 2 of example 3.

Table 4
CPU time comparison between the iterative and direct solvers for example 3

Resolution	CPU time of direct solver (s)	CPU time of iterative solver (s)
11	0.016	0.047
21	0.046	0.063
31	0.063	0.074

iterative or direct solver. Clearly, the CPU time differences will trend to be small with the resolution increasing due to large memory requirement by direct solver. Both iterative and direct solvers can provide the 12-decimal same values when the tolerance of iterative solver is 10^{-12}.

6. Conclusions and remarks

The Chebyshev collocation spectral method for 1D RTE with anisotropic, space-dependent scattering medium is presented, and both iterative and direct solvers are developed. The numerical results for examples with analytical solutions verified the present solvers based on the Chebyshev collocation spectral method can provide exponential space convergence and can capture very large oscillations. Compared with newly appeared methods such as least-square finite elements method (LS or LS-DOM so called), from the formulations and implementations we can conclude that the present method, SP-DOM so called, is simple and efficient.

As to multidimensional problems, the extensions are straightforward. However, as mentioned in the section of introduction, the multidimensional geometries should be regular, and the computer memory should be big enough, especially for participating media. In fact, the authors are developing the spectral cods for 3D problems.

Acknowledgements

This work was supported by the National Fundamental Research Programme of China (No. 2006CB601203). The first author would like to acknowledge Andre Thess and Egbert Zienicke of TU-Ilmenau, who supplied me the chance to learn spectral methods during the period of December 2000 to January 2003. The first author gratefully acknowledges Wai Sun Don, professor of division of applied mathematics, Brown University, who supplied me the subroutine concerned with derivative matrix of Chebyshev spectral collocation method.

References

[1] B.G. Carlson, K.D. Lathrop, Transport theory: the method of discrete ordinates, in: H. Greenspan, C.N. Kelber, D. Okrent (Eds.), Computing Methods in Reactor Physics, Gordon & Breach, New York, 1968.
[2] W.A. Fiveland, Discrete-ordinates solutions of the radiative transport equation for rectangular enclosures, J. Heat Transfer 106 (1984) 699–706.
[3] W.A. Fiveland, Discrete ordinates methods for radiative heat transfer in isotropically and anisotropically scattering media, J. Heat Transfer 109 (1987) 809–812.
[4] W.A. Fiveland, Three-dimensional radiative heat-transfer solutions by the discrete-ordinates method, J. Thermophys. Heat Transfer 2 (1988) 309–316.
[5] R. Siegel, J.R. Howell, Thermal Radiation Heat Transfer, fourth ed., Taylor and Francis, New York, 2002.
[6] M.F. Modest, Radiative Heat Transfer, second ed., Academic Press, San Diego, 2003.
[7] L.A. Gritzo, J.H. Strickland, A gridless solution of the radiative transfer equation for fire and combustion calculations, Combust. Theory Modell. 3 (1999) 159–175.
[8] L.H. Liu, J.Y. Tan, Meshless local Petrov–Galerkin approach for coupled radiative and conductive heat transfer, Int. J. Thermal Sci. 46 (2007) 672–681.
[9] L.H. Liu, J.Y. Tan, Least-squares collocation meshless approach for radiative heat transfer in absorbing and scattering media, JQSRT 103 (2007) 545–557.
[10] Y. Wu, M.F. Modest, D.C. Haworth, A high-order photon Monte Carlo method for radiative transfer in direct numerical simulation, J. Comput. Phys. 223 (2007) 898–922.
[11] J.P. Pontaza, J.N. Reddy, Least-squares finite element formulations for one-dimensional radiative transfer, JQSRT 95 (2005) 387–406.
[12] M. Frank, B. Dubroca, A. Klar, Partial moment entropy approximation to radiative heat transfer, J. Comput. Phys. 218 (2006) 1–18.
[13] B. Chang, A deterministic photon free method to solve radiation transfer equations, J. Comput. Phys. 222 (2007) 71–85.
[14] R.F. Vargas, C.F. Segatto, M.T. Vilhena, Solution of the radiative heat transfer equation with internal energy sources in a slab by the LTSN method, JQSRT 105 (2007) 1–7.
[15] D. Gottlieb, S.A. Orszag, Numerical analysis of spectral methods: theory and applications, Regional Conference Series in Applied Mathematics, vol. 28, SIAM, Philadelphia, 1977.
[16] C. Canuto, M.Y. Hussaini, A. Quarteroni, T.A. Zang, Spectral Methods in Fluid Dynamics, Springer-Verlag, Berlin, 1989.
[17] R. Peyret, Spectral Methods for Incompressible Viscous Flow, Springer, New York, 2002.
[18] F.B. Belgacem, M. Grundmann, Approximation of the wave and electromagnetic diffusion equations by spectral methods, SIAM J. Sci. Comput. 20 (1998) 13–32.
[19] X.W. Shan, D. Montgomery, H.D. Chen, Nonlinear magnetohydrodynamics by Galerkin-method computation, Phys. Rev. A 44 (1991) 6800–6818.
[20] X.W. Shan, Magnetohydrodynamic stabilization through rotation, Phys. Rev. Lett. 73 (1994) 1623–1627.
[21] J.M. Zhao, L.H. Liu, Least-squares spectral element method for radiative heat transfer in semitransparent media, Numer. Heat Transfer B 50 (5) (2006) 473–489.
[22] R. Burke, G.D. Pieter, B. Dennis, Use of fast-Fourier-transform computational methods in radiation transport, Phys. Rev. E 56 (1997) 2217–2227.
[23] D.K. Arnold, I. Akira, A Chebyshev spectral method for radiative transfer equations applied to electromagnetic wave propagation and scattering in a discrete random medium, J. Comput. Phys. 152 (1999) 264–280.
[24] D.K. Arnold, M. Miguel, Chebyshev spectral methods for radiative transfer, SIAM J. Sci. Comput. 23 (2002) 2075–2095.
[25] N. Aouled-Dlala, T. Sghaier, E. Seddiki, Numerical solution of radiative and conductive heat transfer in concentric spherical and cylindrical media, JQSRT 107 (2007) 443–457.
[26] J.P. Boyd, Chebyshev & Fourier Spectral Methods, second ed., Dover, New York, 2001.
[27] B. Fornberg, A Practical Guide to Pseudospectral Methods, Cambridge University Press, Cambridge, 1996.
[28] L.H. Liu, Least-squares finite element method for radiation heat transfer in graded index medium, JQSRT 103 (2007) 536–544.
[29] Y.A. Cengel, M.N. Özişk, Radiation transfer in an anisotropically scattering plane-parallel medium with spacedependent albedo $\omega(x)$, JQSRT 34 (1985) 263–270.
[30] E. Braverman, M. Israeli, A. Averbuch, L. Vozovoi, A fast 3D Poisson solver of arbitrary order accuracy, J. Comput. Phys. 144 (1998) 109–136.
[31] D. Kosloff, H. Tal-Ezer, A modified Chebyshev pseudospectral method with $O(N^{-1})$ time step restriction, J. Comput. Phys. 104 (1993) 457–469.
[32] J.C. Chai, H.S. Lee, S.V. Patankar, Ray effect and false scattering in the discrete ordinates method, Numer. Heat Transfer B 24 (1993) 373–389.
[33] B.W. Li, W.Q. Tao, R.X. Liu, Ray effect in ray tracing method for radiative heat transfer, Int. J. Heat Mass Transfer 40 (1997) 3419–3426.
[34] P.S. Cumber, Ray effect mitigation in jet fire radiation modelling, Int. J. Heat Mass Transfer 43 (2000) 935–943.
[35] B.W. Li, Q. Yao, X.Y. Cao, K.F. Cen, A new discrete ordinates quadrature scheme for three-dimensional radiative heat transfer, J. Heat Transfer 120 (1998) 514–518.
[36] X. Lu, P.F. Hsu, Parallel computing of an integral formulation of transient radiation transport, J. Thermophys. Heat Transfer 17 (2003) 425–433.